Photon-Sail Trajectories Towards Exoplanet Proxima b

Heiligers, M.J.; Rotmans, T.J.

Publication date
2023

Published in
Proceedings of the International Symposium on Space Sailing

Citation (APA)
Heiligers, M. J., & Rotmans, T. J. (2023). Photon-Sail Trajectories Towards Exoplanet Proxima b. In *Proceedings of the International Symposium on Space Sailing*

6th International Symposium on Space Sailing (ISSS 2023), New York, USA, 5-9 June 2023

Photon-Sail Trajectories Towards Exoplanet Proxima b

Tim J. Rotmans[a,*], Jeannette Heiligers[a]

[a]*Department of Astrodynamics and Space Missions, Faculty of Aerospace Engineering, Delft University of Technology, Delft, The Netherlands*

Abstract

This paper investigates trajectories within the Alpha Centauri system to reach planet Proxima b. These trajectories come in the form of connections between the classical Lagrange points of Alpha-Centauri's binary system (composed of the stars Alpha Centauri A and B, AC-A and AC-B) and the classical Lagrange points of the Alpha Centauri C (AC-C)/Proxima b system. These so-called heteroclinic connections are sought using a patched restricted three-body problem method. A genetic algorithm is applied to optimize the linkage conditions between the two three-body systems, focusing on minimizing the position, velocity, and time error at linkage. Four different futuristic, graphene-based sail configurations are used for the analyses: two sails with a reflective coating on only one side of the sail with lightness numbers equal to $\beta = 100$ and $\beta = 1779$, and two sails with a reflective coating on both sides (again, considering $\beta = 100$ and $\beta = 1779$). Results from the genetic algorithm show that, for example, a transfer from the L_2-point in the AC-A/AC-B system to the L_1-point in the AC-C/Proxima b system can be accomplished with a transfer time of 235 years for the one-sided graphene-based sail with $\beta = 1779$.

1. Introduction

While tracking a comet with his telescope in 1689, astronomer Jean Richaud came across the Centaurus constellation. For the first time, he noticed that the star known back then as Alpha Centauri was, in fact, a binary star system [1]. Another 80 years later, in 1915, astronomer Robert T. A. Innes discovered Alpha Centauri C (also referred to as Proxima Centauri) [2], located at 4.25 lightyears from the Solar system, therefore taking on the title of being our closest neighbor. As of today, there is strong evidence that Proxima Centauri is in bound orbit about the binary system [3]. At least two planets are confirmed to be in orbit about Proxima Centauri: Proxima b and Proxima c [4, 5]. One of these two, Proxima b, is a rocky planet in the habitable zone of Proxima Centauri, potentially bearing life. In-situ measurements of Proxima b would provide valuable information in the discussion about life formation on Proxima b and would help our understanding of life formation on rocky exoplanets. A mission to this system is thus endorsed by a strong scientific interest.

The Breakthrough Initiatives have proposed a mission to the Alpha Centauri system using photon sails: Breakthrough Starshot.[1] The aim of this project is to send a swarm of ultra-lightweight sails with gram-sized payloads to Alpha Centauri to perform a flyby of the binary system. Using a 100 GW Earth-based laser array, the sails are propelled to 20% of the speed of light, reaching the system in a little over twenty years. In References [6, 7, 8], several alternative mission scenarios are investigated. Using a futuristic graphene-based sail, the authors studied the possibility of getting captured in the binary system, to then continue towards Proxima Centauri using gravity assists. To get captured in bound orbit about Proxima Centauri, they calculated a maximum arrival speed in the Alpha Centauri A/B system of 5.7% of the speed of light. This results in a 75 years journey from Earth and an additional 46 years towards Proxima Centauri. In Reference [9], comparable results are presented for capture in the Alpha Centauri A-B system using the same sail configuration.

The research presented in this paper focuses on finding photon-sail trajectories starting from the classical colinear Lagrange points in the binary system to the classical colinear and triangular Lagrange points in the AC-C/Proxima b system. As described in previous research [10], the classical triangular Lagrange points are not suited as departure locations in the binary system, because to maintain at the classical Lagrange points, the sail should not create any acceleration. This requires an edge-on position with respect to the incoming sunlight

*Corresponding author, timrotmans@gmail.com

[1] breakthroughinitiatives.org/initiative/3, access date: 18/10/2022

Table 1: Parameters for the three stars within the Alpha Centauri system. The mass, luminosity and radius are expressed in Solar units: $m_\odot = 1.989110 * 10^{30}$ kg, $R_\odot = 6.9598 * 10^5$ km and $L_\odot = 3.854 * 10^{26}$ W [15, 16, 17].

		AC-A	AC-B	AC-C	Sun	Unit
Mass	m	1.100	0.9070	0.1230	1	$m_\odot$
Luminosity	L	1.519	0.5002	0.0015	1	$L_\odot$
Radius	R	1.230	0.8570	0.1450	1	$R_\odot$
Avg. Temperature	T	5790	5260	3040	5770	K

which is not achievable due to the binary star nature of the AC-A/AC-B system. Due to the significant eccentricity of both the AC-A/AC-B system (referred to as the departure system) and the AC-C/Proxima b system (referred to as the arrival system), the elliptic restricted three-body problem (ERTBP) is adopted as dynamical framework. Adequate connections between the two systems are sought by using a patched restricted three-body problem approximation method [11, 12, 13]. In this method, the two systems are "patched" together on a suitable Poincaré section to find a transfer.

The aim is to connect the unstable manifolds of the Lagrange points of the departure system, with the stable manifolds of the Lagrange points in the arrival system. This approach has already proved to be successful for finding transfers between Lagrange points in other photon-sail dynamical systems [13, 14]. To find a proper link between the two systems, the error between the departure and arrival segments of the trajectory at the Poincaré section is evaluated. A numerical optimization problem unfolds in which the error in position, velocity and time is minimized. Similar as in Reference [13], this work uses two techniques to solve this numerical problem. Initial knowledge of the problem is gathered by means of a design space exploration, after which a genetic algorithm is applied to further optimize the link between the systems.

2. Alpha Centauri System

As briefly mentioned in Section 1, Alpha Centauri is a triple star system located at 4.37 light-years from the Sun [15]. In Table 1, some relevant parameters of the stars in the system are given. Figure 1 gives an overview of the orbits of the different bodies in the system. Note that the orbits and the binary system and Proxima b are enlarged to clearly visualize the system. In the center of the system, stars AC-A and AC-B form a binary star system, mutually rotating around the barycenter with a period of approximately 80 years [18]. In reference [19], it is demonstrated with a high degree of confidence that the third star AC-C is in a bound orbit about the binary system. Improved orbital parameters of AC-C's orbit can be found in Reference [20]. The used data is given in the departure observer frame O_d, which is further explained in Section 3.1. AC-C orbits the binary system at approximately 13,000 AU. It is a red-dwarf star with a significantly smaller luminosity and mass than AC-A and AC-B.

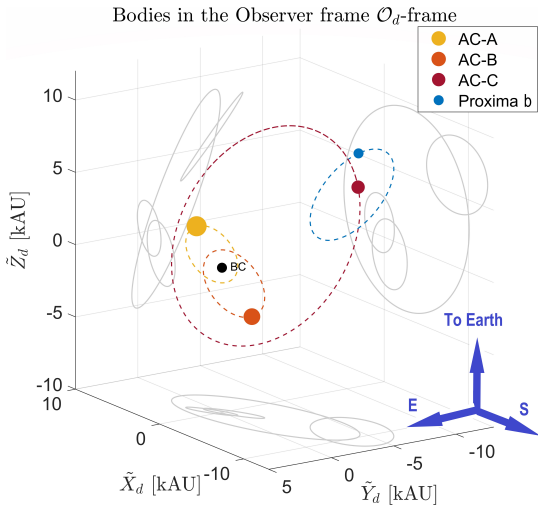

Figure 1: An overview of the positions and orbits of the three stars, including the assumed orbit of Proxima b, at reference epoch J2000. The orbit of AC-C is to scale. The orbits of AC-A and AC-B are enlarged by a factor 200. Proxima b's orbit is enlarged by a factor of 80,000.

Table 2: Orbital elements of Proxima b, AC-A and AC-B [4, 9, 21, 22, 23]. The elements for Proxima b and AC-A/AC-B are given in the observer frame O_a and O_d, respectively.

		Proxima b	AC-A	AC-B	Unit
Semi-major axis	s	0.05	10.79	12.73	AU
Eccentricity	e	0.105	0.52	0.52	-
Inclination	i	Unknown	79.32	79.32	deg
Longitude of the ascending node	Ω	Unknown	205.06	205.06	deg
Argument of periastron	Ψ	310.0	52.0	232.0	deg
Ref. time of periastron	T_0	August 2035	August 2035	August 2035	-

At present, it has been confirmed that two planets are in orbit about AC-C: Proxima b and Proxima c [21, 24]. Only the parameters of Proxima b are presented in Table 2, given in the arrival observer frame O_a, see Section 3.1, since its location and characteristics make it the most interesting of the two. Proxima b is an Earth-like, rocky planet located in the habitable zone. From the data in Table 2 it is clear that there are two unknown orbital elements: the inclination i and right ascension

of the ascending node Ω. However, it is known that Proxima b does not transit AC-C [25], therefore an inclination of close to 90 deg with the plane tangential to the line-of-sight is impossible. Thus, in this work an inclination of $i = 45$ deg is assumed. Based on values presented in [4, 21, 23], the mass of Proxima b, m_{proxb}, is assumed to be 1.3 times that of Earth's mass ($m_\oplus = 5.972 * 10^{24}$ kg).

The reference epoch t_0 used in this paper is August 2035, when AC-A and AC-B are at periastron. Since the true anomaly of Proxima b is unknown, its periastron is set to be at the reference epoch t_0. Note that the period of Proxima b is short (11.186 days), whereas transfer times of hundreds of years are considered reasonable. The assumption on the exact periastron of the arrival system is thus of minor influence on the results. The relationship between the independent variable θ_i and dimensional time t_i, is indirectly given by Kepler's equation [26].

3. Dynamical model

This section provides the dynamical model used and reference frames employed in this work.

3.1. Reference Frames

The following reference frames are used in this research (the corresponding frame transformations can be found in Reference [10]):

1. Inertial frames $\mathcal{I}_d(\mathbf{X}_d,\mathbf{Y}_d,\mathbf{Z}_d)$ (origin in the barycenter of stars AC-A and AC-B) and $\mathcal{I}_a(\mathbf{X}_a,\mathbf{Y}_a,\mathbf{Z}_a)$ (origin in the barycenter of star AC-C and planet Proxima b)
   - $\mathbf{X}_d$, $\mathbf{X}_a$ Aligned with the major axis of the elliptic orbits of the bodies concerned, positive in the direction of AC-B/Proxima b's periastron
   - $\mathbf{Z}_d$, $\mathbf{Z}_a$ Aligned with the angular velocity vector of the system, denoted as $\boldsymbol{\omega}_d$ and $\boldsymbol{\omega}_a$, respectively
   - $\mathbf{Y}_d$, $\mathbf{Y}_a$ Complete the right-handed frames
2. Observer frames $\mathcal{O}_d(\tilde{\mathbf{X}}_d, \tilde{\mathbf{Y}}_d, \tilde{\mathbf{Z}}_d)$ (origin in the barycenter of stars AC-A and AC-B) and $\mathcal{O}_a(\tilde{\mathbf{X}}_a, \tilde{\mathbf{Y}}_a, \tilde{\mathbf{Z}}_a)$ (origin in the barycenter of star AC-C and planet Proxima b)
   - $\tilde{\mathbf{X}}_d$,$\tilde{\mathbf{X}}_a$ Directed towards the intersection between a plane perpendicular to $\tilde{\mathbf{Z}}_d$ or $\tilde{\mathbf{Z}}_a$ and a line through the Celestial Poles.
   - $\tilde{\mathbf{Z}}_d$,$\tilde{\mathbf{Z}}_a$ Aligned with the vector pointing towards the Solar system barycenter
   - $\tilde{\mathbf{Y}}_d$,$\tilde{\mathbf{Y}}_a$ Complete the right-handed frames
3. Rotating pulsating barycentric frames $\mathcal{P}_d(\mathbf{x}_d,\mathbf{y}_d,\mathbf{z}_d)$ (origin in the barycenter of stars AC-A and AC-B) and $\mathcal{P}_a(\mathbf{x}_a,\mathbf{y}_a,\mathbf{z}_a)$ (origin in the barycenter of star AC-C and Proxima b)
   - $\mathbf{x}_d$,$\mathbf{x}_a$ Aligned with the line connecting the two primaries, positive in the direction of AC-B/Proxima b
   - $\mathbf{z}_d$,$\mathbf{z}_a$ Aligned with the angular velocity vector of the system, denoted as $\boldsymbol{\omega}_d$ and $\boldsymbol{\omega}_a$, respectively
   - $\mathbf{y}_d$,$\mathbf{y}_a$ Complete the right-handed frames
4. Sail-centered frames $\mathcal{S}_d(\hat{\mathbf{r}}_A,\hat{\boldsymbol{\theta}}_A,\hat{\boldsymbol{\eta}}_A)$ and $\mathcal{S}_a(\hat{\mathbf{r}}_C,\hat{\boldsymbol{\theta}}_C,\hat{\boldsymbol{\eta}}_C)$ - both with origin in the geometric center of the sail
   - $\hat{\mathbf{r}}_A$,$\hat{\mathbf{r}}_C$ Unit vector from the star (either AC-A or AC-C) to the sail
   - $\hat{\boldsymbol{\theta}}_A = \frac{\mathbf{Z}_d \times \hat{\mathbf{r}}_A}{\|\mathbf{Z}_d \times \hat{\mathbf{r}}_A\|}$, $\hat{\boldsymbol{\theta}}_C = \frac{\mathbf{Z}_a \times \hat{\mathbf{r}}_C}{\|\mathbf{Z}_a \times \hat{\mathbf{r}}_C\|}$
   - $\hat{\boldsymbol{\eta}}_A = \frac{\hat{\mathbf{r}}_A \times \hat{\boldsymbol{\theta}}_A}{\|\hat{\mathbf{r}}_A \times \hat{\boldsymbol{\theta}}_A\|}$, $\hat{\boldsymbol{\eta}}_C = \frac{\hat{\mathbf{r}}_C \times \hat{\boldsymbol{\theta}}_C}{\|\hat{\mathbf{r}}_C \times \hat{\boldsymbol{\theta}}_C\|}$
5. Galactic frames $\mathcal{G}_d(\tilde{\mathbf{x}}_d,\tilde{\mathbf{y}}_d,\tilde{\mathbf{z}}_d)$ (origin in the barycenter of stars AC-A and AC-B) and $\mathcal{G}_a(\tilde{\mathbf{x}}_a,\tilde{\mathbf{y}}_a,\tilde{\mathbf{z}}_a)$ (origin in the center of star AC-C)
   - $\tilde{\mathbf{x}}_d$,$\tilde{\mathbf{x}}_a$ Aligned with a line connecting the Sun with the center of the Milky Way
   - $\tilde{\mathbf{z}}_d$,$\tilde{\mathbf{z}}_a$ Aligned with a vector pointing towards the North Galactic Pole
   - $\tilde{\mathbf{y}}_d$,$\tilde{\mathbf{y}}_a$ Complete the right-handed frame
6. ICRS-frames $\mathcal{E}_d(\mathbf{j}_{d,1}, \mathbf{j}_{d,2}, \mathbf{j}_{d,3})$ (origin in the barycenter of stars AC-A and AC-B) and $\mathcal{E}_a(\mathbf{j}_{a,1}, \mathbf{j}_{a,2}, \mathbf{j}_{a,3})$ (origin in the center of star AC-C). Axes of these frames are defined relative to extragalactic radio sources, see Reference [27].

3.2. Photon-Sail Augmented Elliptic Restricted Three-Body Problem

Due to the large eccentricity of both the departure and arrival systems, the photon-sail augmented elliptic restricted three-body problem is employed. For the equations of motion, the models provided in References [14, 28] are followed. The independent variable is the true anomaly θ_i, where $i = a, d$, referring to variables in the arrival and departure, respectively.. The equations of motion are expressed in the pulsating rotating barycentric frame $\mathcal{P}_i$. The equations of motion are written in

dimensionless form using normalized units: the sum of the two masses as the unit of mass, the distance between the masses as the unit of length, and the inverse of the system's angular velocity $1/\omega_i$ as the unit of time. The mass parameter is introduced, $\mu_i = \frac{m_{2,i}}{(m_{1,i}+m_{2,i})}$, in which $m_{1,i}$ corresponds to the primary with the larger mass, see Table 1. In dimensionless form, the masses become $m_{1,i} = 1 - \mu_i$ and $m_{2,i} = \mu_i$ and these masses are located along the x_i-axis at a distance $-\mu_i$ and $1 - \mu_i$ from the origin, respectively. The period of both systems now becomes 2π.

To model the acceleration from the Solar radiation pressure, an ideal-sail model is used. The ideal-sail model assumes a perfectly flat, specular reflecting sail surface. This means that absorption, re-rediation, and wrinkles in the sail are neglected [29]. This assumption results in a radiation pressure force that is perpendicular to the sail surface, in the direction of the normal vector $\hat{\mathbf{n}}$. The performance of a photon sail can be expressed using its lightness number β [29]. The lightness number is a performance ratio that describes the radiation pressure acceleration relative to the gravitational acceleration of the star that emits the radiation. The relation between the Solar lightness number $\beta_\odot$ and the lightness number relative to another star depends on the mass and luminosity of the respective star [28]. This relation can be expressed as $\beta_k = \epsilon_k \beta_\odot$, with the ratio ϵ_k defined as $\epsilon_k = \frac{L_k m_\odot}{L_\odot m_k}$, see Table 1. The subscript k is used to distinguish between the three stars AC-A, AC-B and AC-C ($k = A, B, C$) The photon-pressure acceleration acting on a sail in a binary-star system is different from that in a single-star system, because in a binary system, the sail will receive radiation emitted by two stars. When considering the binary star system, Eq. 7 given in Reference [28] is used; when the sail is in the AC-C/Proxima b system, the sail acceleration is defined by Eq. 2 in Reference [14]. To potentially increase the capabilities of the sail in the binary system, both a one-sided reflective and a double-sided reflective sail acceleration model are used, as described in Reference [28]. To describe the orientation of the sail with respect to the incoming light, a normal vector $\hat{\mathbf{n}}_k$ is introduced ($k = A, B, C$). The normal vector's direction is expressed by using the cone and clock angles α_k and δ_k. The cone angle is the angle between the normal vector $\hat{\mathbf{n}}_k$ and the local $\hat{\mathbf{r}}_k$-axis. The clock angle is the angle between the $\hat{\boldsymbol{\eta}}_k$-axis and the projection of the normal vector on the plane perpendicular to vector $\hat{\mathbf{r}}_k$ (the $\hat{\boldsymbol{\theta}}_k, \hat{\boldsymbol{\eta}}_k$-plane). The cone and clock angles in the departure system are measured with respect to star AC-A and in the arrival system with respect to star AC-C.

4. Methodology

To design a photon-sail transfer trajectory between AC-A/AC-B and AC-C/Proxima b, a method based on the patched restricted three-body problem approximation [12, 13] is utilized. This section describes this method, as well as an extrapolation method to reduce the computational load associated with the trajectory propagation in the arrival phase, and a brief overview of the optimization problem. The sail configurations analyzed in this study are based on previous research [10]. Four sail configurations (indicated with number 1 to 4) are evaluated: a single-sided and double-sided sail with two different lightness numbers. The lightness numbers for configurations 1 and 2 represent a lower limit that appeared to ensure sufficient acceleration and deceleration during the departure/arrival phases ($\beta = 100$). The lightness numbers for sail configurations 3 and 4 are based on sail configurations previously studied for photon sailing in Alpha Centauri [6] ($\beta = 1779$).

4.1. Patched restricted three-body problem approximation method

The patched restricted three-body problem approximation method used in this work is based on previous studies to find photon-sail transfers between different restricted three-body problems [12, 13]. The unstable manifolds from the colinear Lagrange points in the departure system are used to initiate motion away from the AC-A/AC-B system. In the arrival system, the stable manifolds are exploited to obtain motion towards the Lagrange points. However, the L_4 and L_5-points in the arrival system are stable and do not exhibit manifolds. But, manifolds can be artificially created by exploiting the photon-sail acceleration when the sail is positioned in a non-edge one attitude, which then disrupts the stable motion around the equilibrium. Note that the location of the classical Largange points in the departure and arrival systems are given in Table 5 of Reference [10].

To add flexibility in the design of the transfers, a range of cone and clock angles is considered to create photon-sail assisted unstable and stable manifolds. A constant sail attitude is assumed along these photon-sail assisted manifolds to limit the search space (note that, from here on the addition "photon-sail assisted" is omitted for brevity). Additionally, the non-autonomous nature of the ERTBP adds another dimension to the search space through the time-dependent true anomaly θ_i, at which a trajectory departs or arrives. The resulting manifolds form tube-like structures called photon-sail dedicated sets [12].

The manifolds must then be connected in phase space and time to find a transfer trajectory. A detailed overview of the steps taken to find such transfers, using combinations of sail attitude and departure/arrival time, is given in Reference [10]. In order to evaluate the connection between the photon-sail dedicated sets in phase space, the state of the sail is propagated to a Poincaré section (surface Q). Surface Q is defined in the departure observer frame O_d. It is a section perpendicular to the line connecting the barycenter of the departure system and the barycenter of the arrival system, located exactly halfway along this line. On this surface, the state error, in terms of position, velocity, and time, is evaluated. To reach this surface, the unstable manifolds of the Lagrange points in the departure system are propagated forward in time up to surface Q. In the arrival system, the stable manifolds of the Lagrange points are propagated backwards up to surface Q. These propagations are executed with the ode45 function in Matlab® using relative and absolute tolerances of 10^{-11} and 10^{-11}, respectively The error at surface Q is calculated by comparing the state $\mathbf{x}_{f,d}$ and time $t_{f,d}$ at the end of the unstable manifold with the state $\mathbf{x}_{f,a}$ and time $t_{f,a}$ at the end of the stable manifolds. The magnitude of this error is an indication of the feasibility of the transfer trajectory between the departure and arrival systems. The aim then becomes to find a set of initial/target conditions for the sail that will result in a minimum error (i.e., successful) transfer trajectory. It must be noted that not all initial/target conditions result in a trajectory crossing surface Q. In such a case, the final state of that trajectory will automatically produce a large error, so that the corresponding initial/target conditions are not further considered.

4.2. Arrival system cut-off

A challenge lies in the computation cost associated with the propagation of the stable manifolds in the arrival phase. This computational cost arises from the short period of the arrival system (11.186 days) relative to the total transfer time, which results in the need to propagate the state of the sail over numerous system revolutions, which can be up to thousands. Contrary, the departure system, with a period of approximately 80 years, requires less computational effort. Therefore, based on the research in Reference [10], a linear state extrapolation method is used (also called "cut-off" method) to approximate the state and time of the sail at surface Q without having to propagate the entire (artificial) stable manifold. The method analytically computes the state and time at which the sail reaches surface Q based on the state and time at a predefined cut-off point.

4.3. Optimization problem

The objective of the optimization problem is to minimize the error at linkage as described in Section 4.2. The following sections will further explain the objective function, constraints, and decision variables of this optimization problem.

4.3.1. Objectives

To find a feasible transfer trajectory, three objectives (J_1, J_2 and J_3) are introduced that must be minimized. These objectives are the different errors on the surface Q: position error Δr, velocity error Δv, and time error Δt. The position and velocity errors are calculated using the Euclidean norm difference of the departure and arrival states on surface Q. The time error is calculated in days by subtracting the Julian Date at which the departure phase passes surface Q from the Julian Date at which the arrival phase passes surface Q. It is important to note that the error in sail attitude at surface Q is not considered in the optimization. This means that at surface Q, a sudden, rapid change in sail attitude is allowed. For a real-life mission scenario, the attitude rate of change might be limited and a sudden change not possible. To solve this, a transition phase could be added in between the departure and arrival phase, in which the sail is allowed to slowly change its attitude. To limit the complexity of the computation in this research, such an approach is not used. The impact of this design choice on the final trajectory and results is not expected to be significant.

4.3.2. Constraints

A first set of constraints is defined to prevent that the non-reflective side of the sail faces one of the stars. For all sail configurations these constraints are given as: $\hat{\mathbf{r}}_C \cdot \hat{\mathbf{n}}_C \geq 0$, $\hat{\mathbf{r}}_A \cdot \hat{\mathbf{n}}_A \geq 0$, and $\hat{\mathbf{r}}_B \cdot \hat{\mathbf{n}}_B \geq 0$. To simplify the problem, these constraints are only enforced while the sail remains in the respective systems (departure or arrival) until surface Q is passed. This means, for example, that while the sail trajectory is propagated in the departure system, the back of the sail is allowed to face AC-C. Similarly, in the arrival phase the back of the sail is allowed to face AC-A and AC-B.

Another set of constraints must be enforced to prevent the sail from passing one of the stars too closely. Although a significant sail acceleration can be obtained with close stellar flybys [30], the temperature of the sail can also increase to harmful levels. Therefore, a minimal distance is set to prevent the sail from heating up

too much. Based on values obtained from literature [7], a minimum safe distance of five stellar radii is used in this research: $\mathbf{r}_A > 5 \times R_A$, $\mathbf{r}_B > 5 \times R_B$, and $\mathbf{r}_C > 5 \times R_C$ (where R_k represents the radius of the respective star).

4.3.3. Decision variables

Six variables are defined to tune the trajectories and find a smooth link on surface Q. These six variables (**DV**) are the cone and clock angles during each phase (α_A,δ_A,α_C,δ_C) and the arrival/departure times (t_d and t_a):

$$\mathbf{DV} = \begin{bmatrix} \alpha_A & \alpha_C & \delta_A & \delta_C & t_d & t_a \end{bmatrix} \tag{1}$$

The bounds on the cone and clock angles during both phases are: $-90^\circ \leq \alpha_A, \alpha_C \leq 90^\circ$ and $0^\circ \leq \delta_A, \delta_C \leq 180^\circ$. As described in the introduction, this work is inspired by the Breakthrough Starshot project, which would, in a best-case scenario, launch its sails in 2036, resulting in an arrival at the Alpha Centauri system around 2056. However, it was already shown [3, 9] that to get captured in bound orbit about AC-A or AC-B, which is a necessity when starting from one of the Lagrange points, longer travel times should be expected (up to 80 years). Therefore, it is more reasonable to postpone the time of departure of the mission investigated here to a window in a more distant future. So, the bounds on the departure time from the Lagrange points are set to $01/01/2095 \leq t_d \leq 01/01/2195$. The bounds on the arrival time depend on the sail configuration since a larger lightness number will result in shorter transfer times, and thus, a different arrival window is used for each lightness number ($\beta = 100$ and $\beta = 1779$). For sail configurations 1 and 2 ($\beta = 100$), the arrival time is set to $01/01/3042 \leq t_a \leq 01/01/3122$. For sail configurations 3 and 4 ($\beta = 1779$), the arrival window is bounded as: $01/01/2330 \leq t_a \leq 01/01/2420$. Note that the search space for the departure and arrival time is slightly larger than one period of the departure system. This is intentionally chosen to investigate the impact of the true anomaly at departure, θ_d, on the transfer.

4.4. Optimization methods

In previous work [10], a design space exploration was executed, so that it is possible to limit the design space significantly and obtain initial results for a transfer between the two systems. The conclusions from that design space exploration are briefly summarized here. For sail configurations 1 and 2, using $\beta = 100$, the L_2-point appeared to be the most suitable departure location, and the L_1-point as the most suitable arrival location. For sail configurations 3 and 4, i.e., for $\beta = 1779$, the most optimal departure and arrival locations were L_2 and L_3,

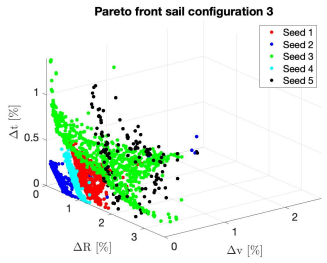

Figure 2: Results from the genetic algorithm for sail configuration 3, where the displays the Pareto front with three objectives using the relative errors.

respectively. In addition, in the current set-up, using a constant sail attitude along the manifolds, the double-sided sail proved to not add any value to solving the problem.

To solve the optimization problem defined in Section 4.3, a genetic algortihm is employed. In particular, Matlab®'s implementation of a multi-objective genetic algorithm *gamultiobj.m* is employed. Three genetic algorithm parameters are tuned to optimize the performance of the algortihm. These parameters are the population size, the number of generations, and the crossover rate. The tuning of these parameters resulted in a population size of 2000, a number of generations of 120, and a crossover fraction of 0.8. To account for the statistical nature of the algortihm, the algorithm is run for five different seeds[2] (with the Mersenne Twister random number generator in Matlab®[3],) to initialize the population. For the sake of simplicity, the seeds in this paper are referred to as seed one to five, while their true values are given in the footnote.

5. Results

This section presents the results of the optimization problem and its implementation described in Section 4. The Pareto fronts for the five different seeds for sail configuration 3 are given in Fig. 2, using relative errors. The relative errors are obtained by dividing the position error Δr by the total distance traveled, the velocity error Δv by the velocity of the sail at surface Q, and the time error Δt by the total travel time of the transfer. The results show that the genetic algorithm is able to converge to solutions that minimize all three objectives effectively. Many solutions fall within a 1-5% error

[2]Seed nrs. (conf. 1): seed 1,2,3,4,5 = [4,12,43,58,12345]. Seed nrs. (conf. 3): seed 1,2,3,4,5 = [4,14,27,55,67]

[3]https://nl.mathworks.com/help/matlab/ref/rng.html, access date 15-02-2023

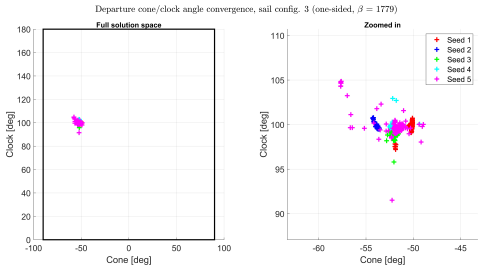

Figure 3: Departure phase: decision variable values (cone and clock angles) of the Pareto front solutions for sail configuration 3.

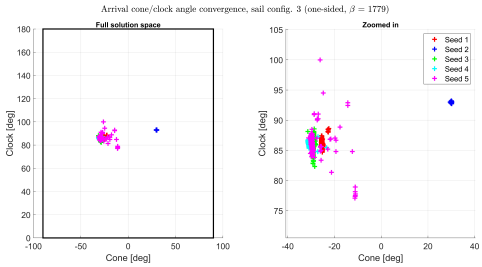

Figure 4: Arrival phase: decision variable values (cone and clock angles) of the Pareto front solutions for sail configuration 3.

margin on all three objectives, and some solutions score even below 1% on all three objectives. This means that the genetic algorithm is able to find a link on surface Q between the departure and arrival phases within reasonable error margins. However, from the Pareto fronts, it can be seen that the quality of the results varies among different seeds. For example, there is a substantial gap in the quality of the results obtained with seed 2 (best Pareto front) and seed 5 (worst Pareto front). This indicates the dependency of the genetic algorithm on the initial population and the algorithm parameter settings, which might be further improved in future research.

In Figs. 3-5, the values of the decision variables corresponding to the Pareto solutions is shown. It is important to note that, although these decision-variable values are plotted separately for the departure and arrival phases (see Figs. 3 and 4), the plots are coupled. The departure phase shows clear convergence to an optimal solution for the cone and clock angles for each seed. All five seeds show convergence to a specific area in the solution space: $-45\,\text{deg} \leq \alpha_d \leq -65\,\text{deg}$, $90\,\text{deg} \leq \delta_d \leq 110\,\text{deg}$. However, the arrival phase shows a less clear area of convergence; from Fig. 5, it can be observed that the algorithm converged to two different regions in the solution space. Only with seed 2 did the algorithm converge to the area with cone angles slightly larger than zero, whereas using the other seeds it converged to cone angles slightly smaller than

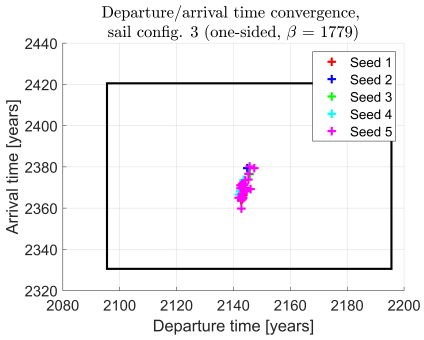

Figure 5: Decision variable values (departure/arrival times) of the Pareto front solutions for sail configuration 3.

zero. Figure 3 already showed that the Pareto front for seed 2 contains much better solutions than for the other seeds. Thus, four out of five seeds got trapped in a local minimum, and, even for seed 2, it is difficult to conclude whether it has converged to a globally optimal solution. Figure 5 shows the final values for the departure and arrival times. Most solutions are in good agreement; the five seeds converged to the same, narrow area: $2140 \leq t_d \leq 2150$, $2360 \leq t_a \leq 2380$. Since the multi-objective optimization results in a 3D Pareto front, no absolute best solution can be selected. However, since the objective is to minimize all three of them, it makes sense to look for a solution in the Pareto front closest to the origin, i.e., the solution (Δr, Δv, Δt) = (0,0,0). Subsequently, the arrival phase is fully propagated to surface Q without employing the "cut-off method" described in Section 4.2, using the initial conditions and sail attitudes corresponding to the optimal solution. This yields the true arrival conditions on the Poincaré surface Q. The resulting trajectories can be found in Reference [10], but the corresponding decision variable values and remaining errors are given in Table 3.

The transfer time found in this research for the solution with the smallest link error (i.e., 235 years for configuration 3, see Table 3) is much longer than results in the literature [7] for a similar sail configuration. In reference [7], a transfer time of 46 years from AC-A/AC-B to AC-C was found. The reason for this shorter transfer time is that, in the cited work, the departure towards AC-C is initiated with a much larger initial velocity. This larger initial velocity results from an interstellar journey at a speed equal to several percentages of the speed of light. However, for the work presented in this paper, the initial inertial velocity depends the on much smaller rotational velocity of the Lagrange points, resulting in much longer transfer times. When adding the

Table 3: Best results from the genetic algorithm for sail configurations 1 and 3. The results give the six decision variables for each phase, as well as the times at linkage $t_{Q,d}$ and $t_{Q,a}$, and link errors.

	Departure loc., arrival loc.	α_d, α_a [deg]	δ_d, δ_a [deg]	t_d, t_a [$yyyy-mm-dd$]	$t_{Q,d}$, $t_{Q,a}$ [$yyyy-mm-dd$]	Transfer time [yrs]	Δr [AU]	Δv [km/s]	Δt [$days$]
Sail conf. 1	L_2,L_1	-56.40, 5.11	98.65, 106.35	2143-02-27, 3168-09-02	2666-11-25, 2667-09-03	1025	70.32	0.236	281.52
Sail conf. 3	L_2,L_3	-53.66, 30.07	99.53, 92.93	2144-11-03, 2379-03-18	2269-03-13, 2268-10-02	235	9.13	0.761	161.08

75-80 years needed to reach AC-A/AC-B from Earth [7] to the 235 year travel time for sail configuration 3 (β = 1779, one-sided), a total mission time of approximately 320 years results. This total mission time includes some margin to maneuver to the L_2 point of the AC-A/AC-B system after the sail's interstellar journey.

6. Conclusion

In this paper, a methodology to compute transfer trajectories from the colinear Lagrange points in the Alpha Centauri A/B (AC-A/AC-B) system to all five Lagrange points of the Alpha Centauri C (AC-C)/Proxima b system has been presented. The photon-sail assisted manifolds originating from the departure Lagrange points and those arriving at the arrival Lagrange points are forwards and backwards propagated up to a suitable Poincaré section where the link errors between the manifolds in terms of position, Δr, velocity, Δv and time, Δt, are evaluated. Results were provided for two particular transfers depending on the lightness number, β, used: 1) For β = 100 from AC-A/AC-B L_2 to AC-C/Proxima b L_1; 2) For β = 1779 from AC-A/AC-B L_2 to AC/Proxima b L_3. The best result for β = 100 showed remaining link errors of: Δr = 70.32 AU, Δv = 0.236 km/s, and Δt = 281.52 days, with a total transfer time of 1025 years, departing in the year 2143 and arriving in 3168. The best result for β = 1779 showed remaining link errors of: Δr = 9.13 AU, Δv = 0.761 km/s, and Δt = 161.08 days, with a total transfer time of 235 years, starting in the year 2144 and arriving in 2379. These errors are small considering the total distance travelled and time passed until reaching the Poincaré section as well as the velocity at the Poincaré section. These results demonstrate that it is most likely possible to find transfers between the Lagrange points of the AC-A/AC-B and AC-C/Proxima b systems with the purpose of, for example, visiting Proxima b. However, starting these transfers to Proxima b from the Lagrange points in the AC-A/AC-B comes at the cost of a much longer travel time than those previously found in literature [7] where the large velocity of the sailcraft after its interstellar journey was exploited to reach Proxima b from AC-A/AC-B in only 46 years.

References

[1] N. Kameswara-Rao et al. Father j. richaud and early telescope observations in india. *Bulletin of the Astronomical Society of India*, 12:81, 1984.

[2] I. S. Glass. The discovery of the nearest star. *African Sky*, 11: 39, 2007.

[3] P. Kervella, F. Thévenin, and C. Lovis. Proxima's orbit around α Centauri. *Astronomy and Astrophysics*, 598, 2017. ISSN 14320746. doi: 10.1051/0004-6361/201629930.

[4] A. Bixel and D. Apai. Probabilistic constraints on the mass and composition of proxima b. 836(2):31, 2017. URL `https://doi.org/10.3847/2041-8213/aa5f51`.

[5] G.F. Benedict and B.E. McArthur. A moving target—revising the mass of proxima centauri c. 4(6):86, jun 2020. URL `https://doi.org/10.3847/2515-5172/ab9ca9`.

[6] R. Heller and M. Hippke. Deceleration of high-velocity interstellar photon sails into bound orbits at Alpha Centauri. *The American Astronomical Society*, 835(2), 1 2017. URL `http://dx.doi.org/10.3847/2041-8213/835/2/L32`.

[7] R. Heller, M. Hippke, and P. Kervella. Optimized Trajectories to the Nearest Stars Using Lightweight High-velocity Photon Sails. *The Astronomical Journal*, 154(3):115, 2017. ISSN 1538-3881. URL `http://dx.doi.org/10.3847/1538-3881/aa813f`.

[8] D.H. Forgan, R. Heller, and M. Hippke. Photogravimagnetic assists of light sails: A mixed blessing for Breakthrough Starshot? *Monthly Notices of the Royal Astronomical Society*, 474(3): 3212–3220, 2018. ISSN 13652966. doi: 10.1093/mnras/stx2834.

[9] F. Schoutetens. Photon-sail trajectory optimization in alpha centauri using evolutionary neurocontrol. Master's thesis, 2019. URL `http://repository.tudelft.nl/`.

[10] T. J. Rotmans. Photon-sail trajectories towards exoplanet proxima b. Master's thesis, Delft University of Technology, Delft, The Netherlands, 2023. URL `http://repository.tudelft.nl/`.

[11] H. Peng et al. Libration transfer design using patched elliptic three-body models and graphics processing units. *Journal of Guidance, Control, and Dynamics*, 40:1–12, 08 2017. doi: 10.2514/1.G002692.

[12] G. Mingotti, J. Heiligers, and C.R. McInnes. First-guess generation of solar sail interplanetary heteroclinic connections. *Advances in the Astronautical Sciences*, 153:1633–1651, 2015. ISSN 00653438.

[13] M. Vergaaij and J. Heiligers. Time-optimal solar sail heteroclinic-like connections for an earth-mars cycler. *Acta Astronautica*, 152, 08 2018. doi: 10.1016/j.actaastro.2018.08.008.

[14] J. Heiligers, G. Mingotti, and C.R. McInnes. Optimal solar sail transfers between halo orbits of different sun-planet systems. *Advances in Space Research*, 55(5):1405–1421, 2015. ISSN 18791948. doi: 10.1016/j.asr.2014.11.033.

[15] P. Kervella et al. A family portrait of the alpha centauri system, 2003. URL `https://www.eso.org/public/news/eso0307/#1`.

[16] F. Thévenin et al. Asteroseismology and calibration of alpha cen

binary system. *Astronomy and Astrophysics*, 392, 2002. doi: 10.1051/0004-6361:20021074.

[17] I.J. Sackmann, A.I. Boothroyd, and K.E. Kraemer. Our sun. iii. present and future. *The Astrophysical Journal*, 418:457–468, 1993.

[18] K. W. Kamper and A.J Wesselink. Alpha and proxima centauri. *The Astronomical Journal*, 83(12):1653–1659, 1978.

[19] P. Kervella et al. Close stellar conjunctions of tauri a and b until 2050 - an mk = 7.8 star may enter the einstein ring of en a in 2028. *Astrodynamics & Astrophysics*, 594:A107, 2016. URL `https://doi.org/10.1051/0004-6361/201629201`.

[20] R. Akeson et al. Precision millimeter astrometry of the centauri ab system. *The Astronomical Journal*, 162, 2021. URL `https://doi.org/10.3847/1538-3881/abfaff`.

[21] A. Suarez Mascareno et al. Revisiting proxima with espresso. *Astronomy Astrophysics*, 639, 2020. URL `https://doi.org/10.1051/0004-6361/202037745`.

[22] G. Anglada-Escudé et al. A terrestrial planet candidate in a temperate orbit around proxima centauri. *Nature*, 536 (7617):437–440, Aug 2016. ISSN 1476-4687. doi: 10.1038/nature19106.

[23] S.R. Kane, D.M. Gelino, and M.C. Turnbull. On the orbital inclination of proxima centauri b. 153(2):52, jan 2017. URL `https://doi.org/10.3847/1538-3881/153/2/52`.

[24] G. Fritz Benedict and Barbara E. McArthur. A preliminary mass for proxima centauri c. 4(4):46, apr 2020. URL `https://doi.org/10.3847/2515-5172/ab84f3`.

[25] E. Gilbert et al. No transits of proxima centauri planets in high-cadence tess data. *Frontiers in Astronomy and Space Sciences*, 8, 2021. doi: 10.3389/fspas.2021.769371.

[26] M. Capderou. *Satellites: Orbits and Missions*. 2005.

[27] G. Kaplan. The iau resolutions on astronomical reference systems, time scales, and earth rotation models. 2006.

[28] J. Heiligers, F. Schoutetens, and B. Dachwald. Photon-sail equilibria in the alpha centauri system. *Journal of Guidance, Control, and Dynamics*, 44(5):1053–1061, 5 2021. ISSN 1533-3884. doi: 10.2514/1.g005446.

[29] C.R. McInnes. *Solar Sailing: Technology, Dynamics, and Mission Applications*. 2 edition, 1999. ISBN 978-1-4471-3992-8. doi: 10.1007/978-1-4471-3992-8.

[30] B. Dachwald. Optimal solar-sail trajectories for missions to the outer solar system. *Journal of Guidance, Control, and Dynamics*, 28(6):1053–1061, 11 2005. doi: 10.2514/1.13301.